Interference effect in the dipole and nondipole anisotropy parameters of the Kr 4*p* photoelectrons in the vicinity of the Kr $(3d)^{-1} \rightarrow np$ resonant excitations

S. Ricz,[1,2] T. Ricsóka,[1,2] K. Holste,[2] A. Borovik Jr.,[2] D. Bernhardt,[2] S. Schippers,[2] Á. Kövér,[1] D. Varga,[1] and A. Müller[2]

[1]*Institute of Nuclear Research of Hungarian Academy of Sciences, Debrecen, P.O. Box 51, H-4001, Hungary*

[2]*Institute for Atomic and Molecular Physics, Justus-Liebig University Giessen, D-35392 Giessen, Germany*

(Received 21 January 2010; published 26 April 2010)

The angular distribution of the Kr 4*p* photoelectrons was investigated in the photon energy range of the $(3d)^{-1} \rightarrow np$ resonant excitations. The experimental dipole (β) and nondipole (γ and δ) anisotropy parameters were determined for the spin-orbit components of the Kr 4*p* shell. A simple theoretical model was developed for the description of the photoionization and excitation processes. An interference effect was observed between the direct photoionization and the resonant excitation participator Auger decay processes in the photon energy dependence of the experimental anisotropy parameters.

DOI: 10.1103/PhysRevA.81.043416 PACS number(s): 32.80.Fb, 32.80.Aa

I. INTRODUCTION

The interference between the direct photoionization and the resonantly excited participator Auger decay has been investigated only in the past few years [1–3]. Whitfield *et al.* [1] studied the angular distribution of the Kr 4*s* and Xe 5*s* photoelectrons both theoretically and experimentally in the photon energy range of the Kr $(3d)^{-1} \rightarrow np$ (90 eV$\leqslant h\nu \leqslant$95 eV) and the Xe $(4d)^{-1} \rightarrow np$ (64 eV$\leqslant h\nu \leqslant$69.5 eV) resonant excitations. The energy dependence of the experimental cross sections and dipole anisotropy parameters (β) showed a clear resonant structure in the investigated photon energy range. The energy dependence of the measured β parameters were compared with the data of the relativistic random-phase approximation (RRPA) and the relativistic multichannel quantum defect (RMQDT) calculation. Both the experiment and the RRPA approximation showed a "surprising deviation" from the expected $\beta = 2$ value and the agreement was good between the two data sets for the off resonant photon energies. The RMQDT description could reproduce only qualitatively the resonant structure of the measured dipole parameter.

Gorczyca and Robicheaux [2] described the Ar 3*s*- and 3*p*-shell photoionization in the framework of the RMQDT calculation in the photon energy region 244–251 eV of the $(2p)^{-1} \rightarrow ns/md$ resonant excitations. The cross sections as well as the dipole anisotropy parameters were calculated for both outer shells of Ar. They found good agreement between the calculated and the measured resonance profiles of the $(3s)^{-1}$ and $(3s+3p)^{-1}+(3p)^{-2}nl$ relative cross sections. The theoretical dipole β parameter could not be compared with any experiment due to the lack of experimental data at the time. The calculated dipole parameter showed a strong interference between the direct photoionization and the participator resonant Auger decay. Furthermore, its photon energy dependence was different for the fine structure components of the Ar 3*p* shell indicating a strong spin-orbit effect.

In our earlier article [3] the experimental dipole and nondipole (γ and δ) anisotropy parameters were reported for the fine structure components of the Ar 3*p* photoelectrons in the photon energy range of the $(2p)^{-1} \rightarrow ns/md$ resonant excitations. The experimental and the theoretical [2] dipole parameters were in good agreement. This confirmed experimentally the existence of interference between the direct and nondirect photoionization processes and the importance of spin-orbit effects. The measured nondipole anisotropy parameters also showed an indication of interference, however, due to experimental uncertainties this result was not fully conclusive.

In the present work the interference effect between the direct and indirect photoionization was investigated with the method of angle-resolved photoelectron spectroscopy. The angular distribution of 4*p* photoelectrons of krypton was measured with linearly polarized synchrotron radiation in the photon energy range (89.85–94.4 eV) of the $(3d)^{-1} \rightarrow np$ resonant excitations in order to determine the dipole (β) and nondipole (δ and γ) angular anisotropy parameters. The experimental dipole β parameters were compared with a simple theoretical estimation based on hydrogenic and Coulomb wave functions for the bound and free electrons, respectively.

II. EXPERIMENT

The experiment was performed at the beam line BW3 of the third generation DORIS III storage ring at HASYLAB, Hamburg, Germany [4–7]. The operating energy of this synchrotron is 4.45 GeV and both electrons and positrons can be used for creating synchrotron radiation. The photon source of the beam line BW3 is a combination of two undulators. The photon beam is monochromatized with a SX-700 grating monochromator. The photon energy range is 20–2000 eV. The photon flux was measured by a photodiode. The linear polarization of the photon beam was monitored by recording the angular distribution of the Ne 2*s* photoelectrons at 250 eV photon energy where the nondipole contribution is negligible [8]. The radiation was found to be completely linearly polarized: 100% within 2% uncertainty.

The emitted electrons were analyzed using the ESA-22D electrostatic electron spectrometer. The spectrometer consists of a spherical and a cylindrical mirror analyzer. The spherical mirror focuses the electrons from the scattering plane to the entrance slit of the cylindrical analyzer which then performs the energy analysis of the electrons. A detailed description of an ESA-22 type analyzer is presented in Ref. [9]. A spherical deceleration lens is placed around the source region to improve the energy resolution of the system. The analyzer and the

interaction region is lined with two layers of μ-metal sheets and the residual magnetic field is less than 5 mG in the scattering plane and in the analyzer. The photoelectrons were detected by 22 channeltrons in coplanar geometry, i.e., in the polarization plane at $\phi = 0^\circ$ azimuthal angle and at 22 polar angles between 0° and 360° (except 90° and 180°) relative to the polarization vector. The angular window of each channeltron was $\pm 1.7^\circ$ in vertical and $\pm 5^\circ$ in horizontal directions.

The relative efficiencies of the detectors were determined by measuring the angular distribution of Ne $2s$ photoelectrons ionized by 131.8-eV photons. At this photon energy the theoretical estimations for the dipole and nondipole anisotropy parameters are $\beta = 1.9996$ and $\gamma = -0.0019$ in the frame of relativistic independent particle model [10] and $\gamma = -0.0034$ in random-phase approximation [11] (the β parameter was not calculated). On the basis of these estimations, using the above parameters, the detector efficiencies can be determined by fitting Eq. (1) (see below) to the measured angular distribution of Ne $2s$ photoelectrons. The difference between the two γ values is used as systematic error. Note that the δ nondipole parameter is zero for s shells. The efficiencies of the detectors were measured before and after the injection of positrons into the DORIS III storage ring to take into account the effect of possible beam movement on the sensitive area of the spectrometer.

The angular distribution of Kr $4p$ photoelectrons was measured at 30-eV pass energy and with 100-μm photon monochromator slit size. As a result, the full width at half maximum (FWHM) of the electron spectrometer was 68 meV and the photon bandwidth was approximately 20 meV in the $(3d)^{-1} \rightarrow np$ resonant excitation range. These settings ensured the separation of spin-orbit components of Kr $4p$ photoelectron lines.

The angular anisotropy parameters of Kr $4p$ photoelectrons were obtained from the fit of the efficiency corrected experimental intensities according to the following equation [12]

$$\frac{d\sigma_{nlj}}{d\Omega} = \frac{\sigma_{nlj}}{4\pi}\{1 + \beta P_2(\cos\theta) + [\delta + \gamma\cos^2(\theta)]\cos(\phi)\sin(\theta)\}, \tag{1}$$

where P_2 is the second-order Legendre polynomial, σ_{nlj} is the photoionization cross section of the nlj orbital, β is the anisotropy parameter of the dipole interaction ($E1$), γ and δ are the parameters related to the nondipole interactions ($E1 \otimes E2, M1$), whereas θ and ϕ define the polar and azimuthal angles relative to the polarization vector, respectively. This formula describes the angular distribution of photoelectrons ejected from a randomly oriented sample by 100% linearly polarized light. In the present setup the angular distribution of the photoelectrons was collected in the oscillation plane of the electric field of the incoming photon beam. This means that the dipole and nondipole parameters can be determined from the same angle-resolved spectrum.

III. THEORETICAL ESTIMATION

In this section a simple theoretical model is presented for the photoeffect (ionization or excitation, IE) using the nonrelativistic dipole approximation and independent particle model (IPM) for closed shell atoms. The following processes are included in the theoretical estimation

$$\begin{aligned} h\nu + A &\rightarrow A^+(4p)^{-1} + e_{\text{photo}} \\ h\nu + A &\rightarrow A^*[(3d)^{-1}n'p] \rightarrow A^+(4p)^{-1} + e_{\text{p-Aug}}, \end{aligned} \tag{2}$$

where the first line designates the direct photoionization, the second one shows the resonant photoexcitation-participator Auger decay, and n' and p are the principal and angular-momentum quantum numbers of the excited electron. The second process is possible only when the photon energy equals the $(3d)^{-1} - n'p$ excitation energy and the energy of the participator Auger electrons $e_{p\text{-Aug}}$ is the same as the emitted photoelectrons e_{photo} in the first line of Eq. (2).

In this model we assumed that the direct photoionization and resonant excitation exclude each other and the resonances are discrete (energetically no overlap of the resonant states). The total transition amplitude (i.e., the sum of the individual matrix elements) is

$$M_{nl}^{\text{ion+exc}} = \sum_{l',l''=|l-1|}^{l+1} \left\{ M_{nl,l''}^{\text{ion}} + \sum_{n'=n+1}^{\infty} M_{n'l'}^{\text{exc}} \right\}, \tag{3}$$

where $M_{nl}^{\text{ion+exc}}$, $M_{nl,l''}^{\text{ion}}$, and $M_{n'l'}^{\text{exc}}$ denote the resultant and the partial matrix elements of the ionization and excitation processes; n, n' are the principal quantum numbers of the ionized atomic shell and the excited electron; and l, l', and l'' mark the angular momenta of the ionized atomic shell of the excited states and of the emitted photoelectrons, respectively. Considering the nonrelativistic dipole approximation the ionizations and excitations are described by two partial waves. In this case Eq. (3) can be separated

$$\begin{aligned} M_{nl}^{\text{ion+exc},<} &= M_{nl,l-1}^{\text{ion}} + w_1 \sum_{n'=n+1}^{\infty} \sum_{l'=|l-1|}^{l+1} M_{n'l'}^{\text{exc}} \\ M_{nl}^{\text{ion+exc},>} &= M_{nl,l+1}^{\text{ion}} + w_2 \sum_{n'=n+1}^{\infty} \sum_{l'=|l-1|}^{l+1} M_{n'l'}^{\text{exc}}, \end{aligned} \tag{4}$$

where $<$ and $>$ denote the $l-1$ and $l+1$ partial waves of the emitted photoelectrons. w_1 and w_2 are the mixing coefficients between the ionization and excitation channels and their sum is unity. In the present work the statistical weights were used, i.e., the excitation amplitudes were weighted with the angular momenta of the photoelectron, namely

$$\begin{aligned} w_1 &= \frac{2|l-1|+1}{2|l-1|+1+2(l+1)+1} \\ w_2 &= \frac{2(l+1)+1}{2|l-1|+1+2(l+1)+1}. \end{aligned} \tag{5}$$

On the grounds of the above-mentioned model, the present calculation is based on the articles of Kennedy and Manson [13], Tseng *et al.* [14], and Cooper [12] (atomic units are used). The differential cross section for the photoeffect is

$$\frac{d\sigma_{nl}}{d\Omega} = \frac{\sigma_{nl}}{4\pi}\{1 + \beta_{nl} P_2(\cos\theta)\} \tag{6}$$

in dipole approximation for linearly polarized photons. σ_{nl} is the total photoionization and excitation cross section for the nl subshell of the atom, β_{nl} is the corresponding dipole anisotropy parameter, P_2 is the second-order Legendre polynomial, and

θ is the polar angle between the polarization vector of the photons and the momentum of photoelectrons. The total cross section σ_{nl} is the following [12]

$$\sigma_{nl} = \frac{4\pi^2\alpha}{3(2l+1)} N_{nl}\omega\left[l R^2_{\omega,l-1} + (l+1)R^2_{\omega,l+1}\right] \quad (7)$$

for closed-shell atoms. In Eq. (7) α is the fine structure constant, $R_{\omega,l\pm1}$ is the radial part of the dipole matrix element, ω is the photon energy, and N_{nl} is the number of the electrons on the nl atomic shell. The dipole anisotropy parameter β_{nl} can be expressed as [12]

$$\beta_{nl} = \frac{l(l-1)R^2_{\omega,l-1} + (l+1)(l+2)R^2_{\omega,l+1} - 6l(l+1)R_{\omega,l-1}R_{\omega,l+1}\cos(\delta_{l+1}-\delta_{l-1})}{(2l+1)\left[l R^2_{\omega,l-1} + (l+1)R^2_{\omega,l+1}\right]} \quad (8)$$

for randomly oriented closed-shell atoms. The Coulomb phase shift δ_l [15] for an ion with nuclear charge Z is defined by

$$\delta_l = \arg\Gamma\left[l+1-i\left(\frac{Z-N}{p}\right)\right]. \quad (9)$$

Here N is the number of bound electrons, p is the momentum of the photoelectron, and Γ is the gamma function [16]. The dipole radial matrix element is

$$R_{\omega,l'} = \int_0^\infty R_{n'l'}(r) r^3 R_{nl}(r) dr \quad (10)$$

in length form. $R_{nl}(r)$ is the initial radial wave function of the bound state and $R_{n'l'}(r)$ represents the final-state radial wave function with $l' = l \pm 1$. n' denotes the principal quantum number for photoexcitation or the energy of the emitted photoelectrons for photoionization. In the latter case the wave function is normalized to unit energy interval.

In velocity form the radial matrix element can be expressed as

$$R_{\omega,l'} = \frac{1}{E_n - E_{n'}} \int_0^\infty \left\{ R_{n'l'}(r) r^{-1} R_{nl}(r)[l'(l'+1) - l(l+1)] - 2R_{n'l'}(r)\frac{dR_{nl}(r)}{dr} \right\} r^2 dr, \quad (11)$$

where E_n and E'_n are the energies of the system in initial and final states, respectively. Substituting the appropriate radial matrix element [Eq. (10) or Eq. (11) for ionization and excitation, respectively] into Eq. (4), the dipole radial transition amplitudes of photoionization or excitation (IE) processes can be computed in both length and velocity forms.

In the present calculation the initial and final bound states were represented by hydrogen-like wave functions while the continuum states were described by Coulomb wave functions [16]. For the $4p$ ground and the $(3d)^{-1} \rightarrow np$ excited states of Kr the effective nuclear charges were determined from the experimental binding energies [10,17]. The photon energies for resonant excitation were obtained from the experimental data of King *et al.* [17]. These values were used in the calculation of the hydrogen-like radial wave functions and transition matrix elements for photon impact.

For testing the present description the Kr $4p$ IE cross sections were calculated in both length and velocity forms. Figure 1 shows the comparison between the experimental and different theoretical data as well as our estimation in the photon energy range of the $(3d)^{-1} \rightarrow np$ resonant excitations for Kr $4p$ photoelectrons. Our calculated data were convoluted with a FWHM = 80 meV wide Lorentz function to account for the natural width of the resonances [17]. The experimental cross sections for direct $4p$ ionization were derived from the measurement of Aksela *et al.* [18] with a linear interpolation. This approximation should be good due to the flatness of the measured data which were measured only at those energies where there are no resonances. One can see there is no contradiction between the present estimation and the earlier theoretical calculations [19,20] within the theoretical uncertainties (typically a factor of 2 for absolute cross sections). The difference between the length and the velocity cross sections originates from the used simple wave functions. The two forms should produce the same results only for the exact eigenfunctions (for details see Ref. [21]). However, the present calculation demonstrates that the contribution of the excitation to the cross section is not negligible even in the framework of the independent particle model. In the next section the effect of the IE process will be presented for the dipole angular anisotropy parameter of the Kr $4p$ photoelectrons and compared with the experiment.

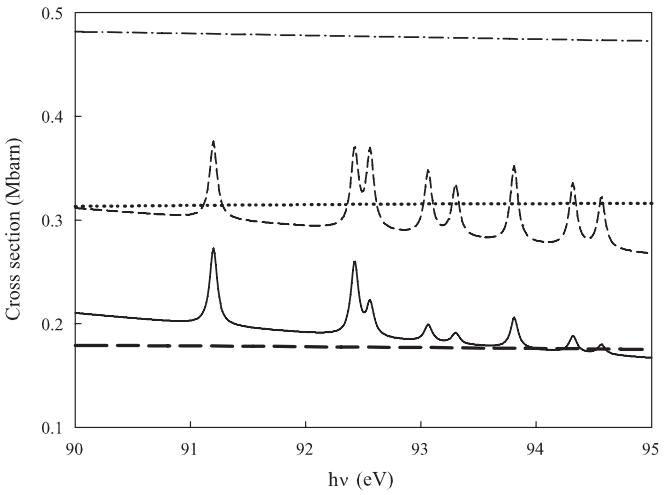

FIG. 1. Kr $4p$ photoionization cross section as a function of photon energy in the $(3d)^{-1} \rightarrow np$ resonant excitation range. The dashed and solid lines show the present calculation in length and velocity forms, respectively. The dashed-dotted line is the experimental data (interpolated from Aksela *et al.* [18]). The thick long dashed and dotted lines are the multichannel [19] and the RRPA calculations [20], respectively.

IV. RESULTS AND DISCUSSION

Figures 2, 3, and 4 show the measured dipole and nondipole anisotropy parameters of the Kr $4p$ photoelectrons. The figures demonstrate well that the resonant excitations modify the angular distribution of the photoelectrons in the investigated photon energy range. For example, the experimental dipole β parameters vary between 0.7 and 1.4 [see Fig. 2(a) and top panels in Figs. 3 and 4] what is in strong contrast to the observation of Whitfield *et al.* [1] for Kr $4s$ photoelectrons in the same energy range. This is not surprising because Eq. (8) yields $\beta = 2$ for $l = 0$ independent of the dipole matrix element (due to the single p-partial wave emission). Any difference from $\beta = 2$ is a signature of a many electron phenomenon such as electron correlation, interaction among different ionization/excitation channels, and so on.

The situation differs completely for the $p, d, f, \ldots$ shells where β according to Eq. (8) depends explicitly on the radial dipol matrix elements $R_{\omega,l\pm1}$. Figure 2(a) shows the comparison between the experimental and the calculated dipole anisotropy parameters for the Kr $4p$ shell (solid and dashed lines represent the velocity and the length forms). Both the measured and the theoretical data show a peaklike structure at all $(3d)^{-1} \rightarrow np$ resonant excitation photon

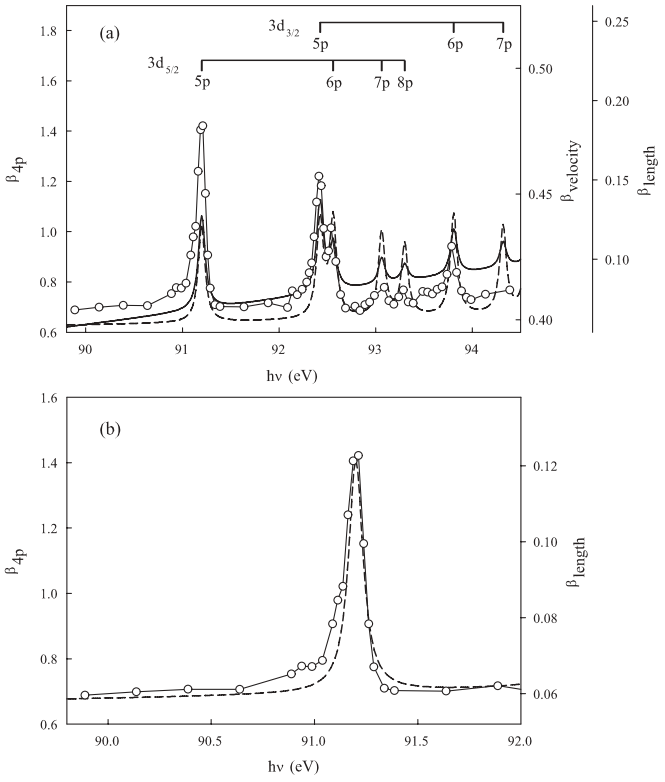

FIG. 2. Kr $4p$ dipole anisotropy parameters as a function of the photon energy in the $(3d)^{-1} \rightarrow np$ resonant excitation range (a). Open circles with connection line is the result of the present experiment; the dashed and solid lines denote our calculation in length and velocity forms (right hand scales). The vertical bars with assignments represent the energy positions and the names of the resonances. The bottom figure (b) shows a part of the top one around the $(3d_{5/2})^{-1} \rightarrow 5p$ resonant excitation with the length form calculation (dashed line and right scale).

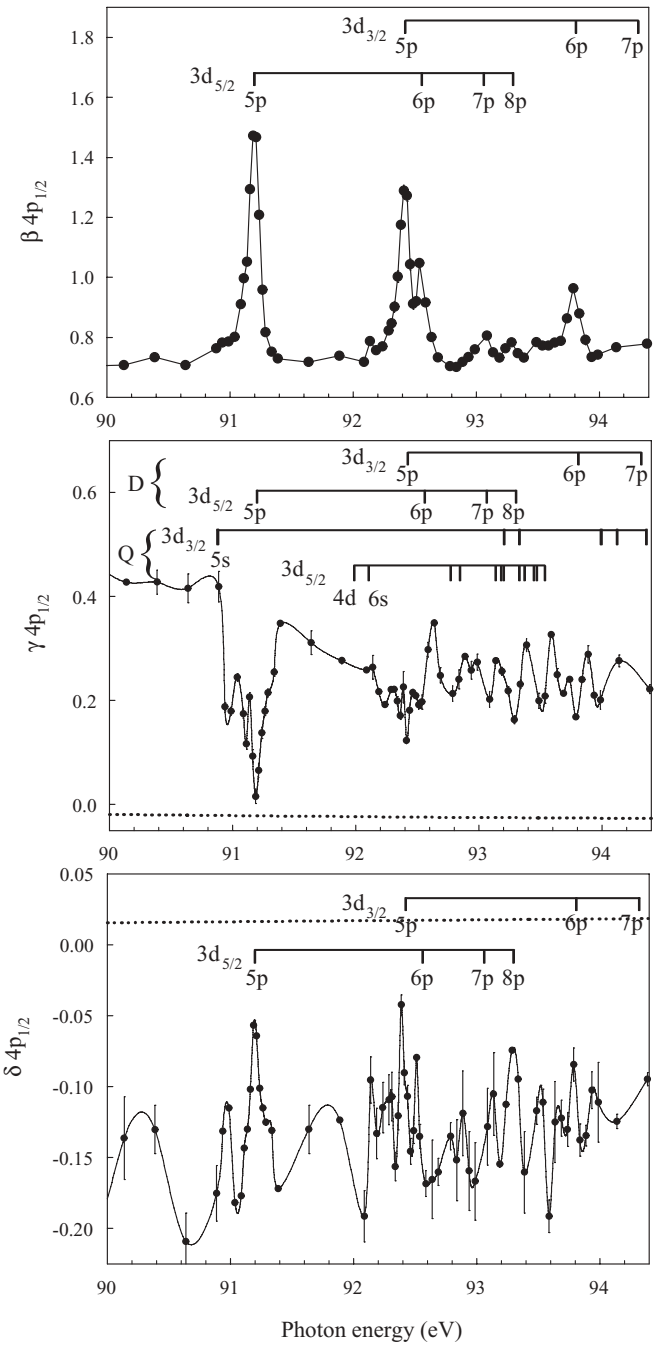

FIG. 3. Experimental dipole β (top panel), nondipole γ (middle panel), and δ (bottom panel) anisotropy parameters for the Kr $4p_{1/2}$ photoelectrons in the $(3d)^{-1} \rightarrow np$ resonant excitation photon energy range. The dotted lines on the middle and bottom panels are the RRPA calculation of Banerjee *et al.* [22]. The vertical bars with assignments show the energy position and the name of the resonances. D and Q denote the dipole and quadrupole allowed transitions on the middle panels.

energies (vertical bars). The nonrelativistic IPM approximation predicts also a non-negligible contribution to the anisotropy parameters from the resonant excitation in agreement with the experiment. The theoretical description of the IE process could reproduce the measured structure qualitatively but the quantitative agreement is very poor (see Fig. 2 and

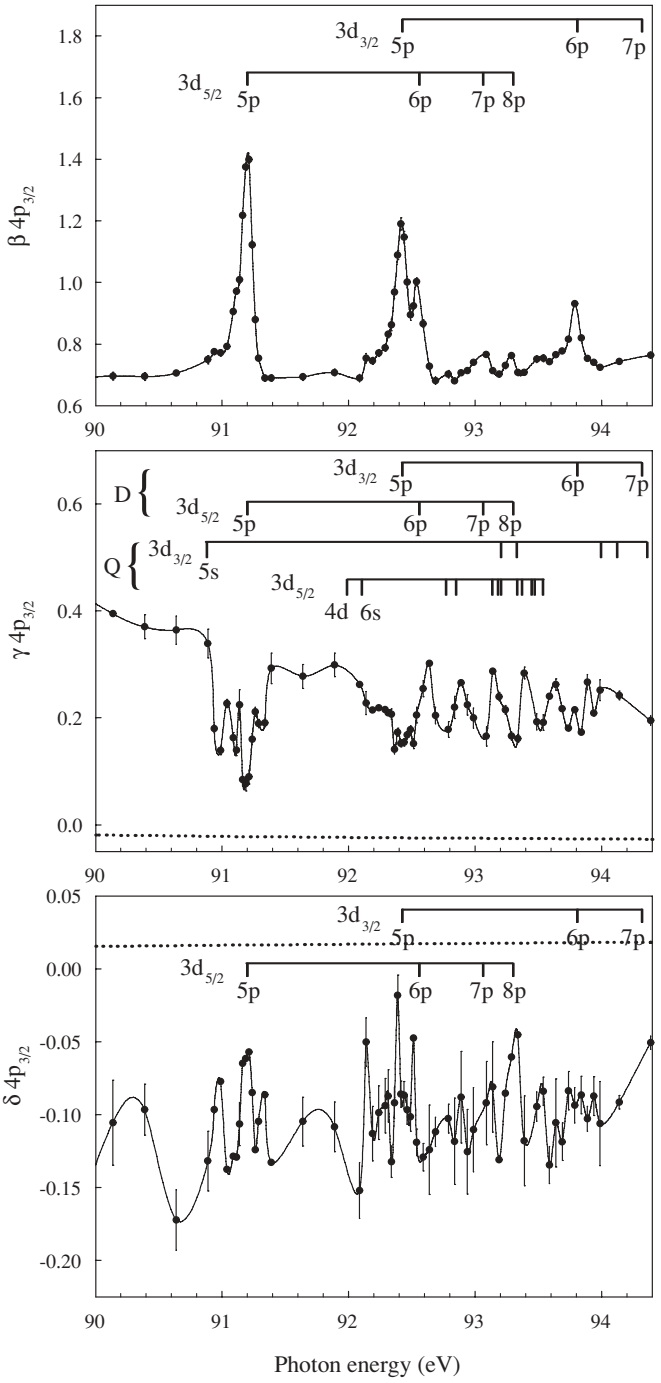

FIG. 4. The same as Fig. 3 for the $4p_{3/2}$ photoelectrons.

Table I). This disagreement is not surprising because of the simplicity of the model. Figure 2(b) displays the β parameters around the $(3d_{5/2})^{-1} \rightarrow 5p$ resonant excitation together with the present calculation (dashed line in length form). It can be seen that the photon energy dependence of the measured data differs from the theoretical one. The experimental peaklike structure has a Fano-profile shape, i.e., it shows a long tail in the low-energy side and drops down rapidly above the resonant energy, while the calculated shape is symmetric. The measured asymmetric distribution demonstrates the breakdown of the independent particle model. This effect is visible also for the dipole parameters of the spin-orbit components of the $4p$ shell on the top panels of Figs. 3 and 4. However, the present measurement shows a smaller difference between the $4p_{1/2}$ and $4p_{3/2}$ fine-structure components of Kr (see Fig. 5 for the ratios of the experimental β parameters) than it was observed for the Ar $3p$ shell [3]. The $\beta_{1/2}/\beta_{3/2}$ ratio is approximately 1.03 in the off-resonant photon energy regions and it grows up to $\beta_{1/2}/\beta_{3/2} \approx 1.1$ around the strong $(3d_{3/2,5/2})^{-1} \rightarrow 5p, 6p$ resonances. A possible interpretation of the observed asymmetry is the interference between the direct photoionization and the resonantly excited participator Auger decay. The difference between the of-f and on-resonance ratios shows a weak influence of the spin-orbit interaction in this interference effect.

For the experimental nondipole parameters (γ and δ) the effect of the $3d$ excitations is not as visible as for the dipole parameter β (see the middle and the bottom panels in Figs. 3 and 4). However, around the strongest $(3d_{3/2,5/2})^{-1} \rightarrow 5p$, $6p$ resonances a valley and a weak peaklike structure can be seen for the γ and δ parameters. Figures 3 and 4 display the comparison of the experimental data with the RRPA calculation of Banerjee *et al.* [22] for the nondipole parameters (γ and δ, dotted lines in the middle and bottom panels). The measured data differ from the theory both in magnitude and in sign. This discrepancy may be interpreted with the neglect of the resonant excitation channels in the RRPA description.

An important difference between the dipole β and nondipole γ parameters is the width of the contribution of the $3d$ excitations to the anisotropy parameters. The experimental width of the $(3d_{5/2})^{-1} \rightarrow 5p$ resonant excitation is approximately 110 meV for β while it is 440 meV for the γ parameter. This big difference may originate from some quadrupole allowed resonant photoexcitation. A similar effect was observed by Krässig *et al.* [23] for He and was predicted theoretically by Dolmatov and Manson [24] for Mn. The energies of the Kr $3d_{3/2,5/2} \rightarrow ns/nd/ng$ quadrupole excitations were calculated (E_{th}) and the results are presented in Table II. The calculations were performed by using the Hartree-Fock method with relativistic corrections [25]. The theoretical energies were shifted by 0.698 eV to reproduce the experimental energy for the $(3d_{5/2})^{-1} \rightarrow 4d$ transitions

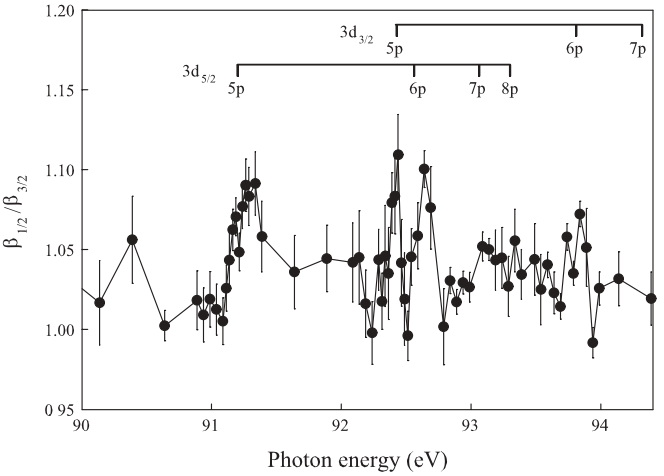

FIG. 5. Photon energy dependence of the experimental $\beta_{1/2}/\beta_{3/2}$ ratios for the $4p_{1/2}$ and $4p_{3/2}$ photoelectrons of krypton.

TABLE I. Comparison between the measured and calculated dipole anisotropy parameters β_{4p} for krypton $4p$ shell at the $(3d_{3/2,5/2} \rightarrow np)$ resonant photon energies. The resonant energies $h\nu$ are from Ref. [17] and exp., length and velocity denote the experiment and the theoretical estimations in length and velocity forms, respectively. The bottom part of the table shows the off resonant dipole parameters at three photon energies.

	β_{4p}							
	$3d_{5/2}$				$3d_{3/2}$			
Excited state	$h\nu$ (eV)	Exp.	Length	Velocity	$h\nu$ (eV)	Exp.	Length	Velocity
$5p$	91.20	1.414(3)	0.122	0.441	92.43	1.221(5)	0.129	0.448
$6p$	92.56	1.015(3)	0.130	0.432	93.81	0.942(2)	0.129	0.436
$7p$	93.06	0.779(2)	0.119	0.425	94.32		0.122	0.431
$8p$	93.30	0.769(3)	0.111	0.423	94.57		0.113	0.429
Off resonance	89.89	0.689(4)	0.059	0.398				
β_{4p}	91.64	0.701(3)	0.062	0.407				
	94.39	0.768(2)	0.082	0.4241				

[17]. The other experimental excitation energies (E_{exp}) were measured by Yuan *et al.* [26] (Table II) and the agreement with the calculated one is excellent within the experimental uncertainties. One can see that only the $(3d_{3/2})^{-1} \rightarrow 5s$ and $(3d_{5/2})^{-1} \rightarrow 6s$ quadrupole resonances are close to the $(3d_{5/2})^{-1} \rightarrow 5p$ and $(3d_{3/2})^{-1} \rightarrow 5p$ dipole excitations. However, the observed broadening cannot be explained with these two quadrupole resonances due to the fact that the energy differences between the dipole and quadrupole transitions are larger (≈320 meV, see middle panel in Figs. 3 and 4) than their natural widths. The widths of the dipole and quadrupole resonances are approximately the same (80–90 meV, see Refs. [17,26]). Therefore, they can produce only an extra structure in the γ spectrum in the low-energy side of the "γ minima" as it was observed for He in Ref. [23]. The broadening observed in the present experiment might be explained by the interactions among the different ionization processes next to the excitation channels in the electric quadrupole matrix elements. A similar effect was found for the Xe $5s$ photoionization around the $4p$ ionization threshold [27,28].

We cannot make any definite statement for the measured δ nondipole parameters due to the experimental uncertainties. However, a peaklike structure can be seen in the δ spectrum at the $(3d_{3/2})^{-1} \rightarrow 5s$ (around 91 eV) and at the $(3d_{5/2})^{-1} \rightarrow 5p$ (91.2 eV) resonant excitations (see bottom panel of Figs. 3 and 4). This indicates that the magnetic dipole interactions are not negligible in the interference between the direct ionization and the resonantly excited participator Auger decay processes.

Figure 6 shows the experimental intensity ratios for the $4p_{3/2}$ ($I_{3/2}$) and $4p_{1/2}$ ($I_{1/2}$) photoelectrons of krypton in the investigated photon energy range. These ratios should be independent of the photon energy and the coupling scheme (e.g., the ratio is 2 in LS coupling). Any difference from a constant value clearly demonstrates the presence of the interference among the direct and one or more indirect ionization channels. The observed structures confirm that the interference effect is not negligible between the resonant excitation and photoionization processes. Local maxima and

TABLE II. Krypton $3d_{3/2,5/2} \rightarrow ns/nd/ng$ quadrupole resonant excitation energies calculated with the Hartree-Fock method with relativistic corrections [25] (E_{th}). The given energies are shifted by 0.698 eV to fit the experimental $4d$ excitation energies of King *et al.* [17]. The measured excitation energies are from Ref. [26] (E_{exp}).

	$3d_{5/2}$		$3d_{3/2}$	
Excited state	E_{th} (eV)	E_{exp}[a] (eV)	E_{th} (eV)	E_{exp}[a] (eV)
$5s$	89.658	89.64(1)	90.880	90.89(2)
$6s$	92.105	92.09(2)	93.330	
$7s$	92.849	92.86(2)	94.123	
$8s$	93.181		94.407	
$4d$	91.987[b]	91.99(2)	93.206	
$5d$	92.771	92.78(2)	93.994	94.04(3)
$6d$	93.136		94.361	
$7d$	93.331		94.556	
$8d$	93.446		94.671	
$5g$	93.204		94.431	
$6g$	93.371		94.597	
$7g$	93.471		94.697	
$8g$	93.536		94.762	

[a]From Ref. [26].

[b]Experimental energy from Ref. [17] for normalization.

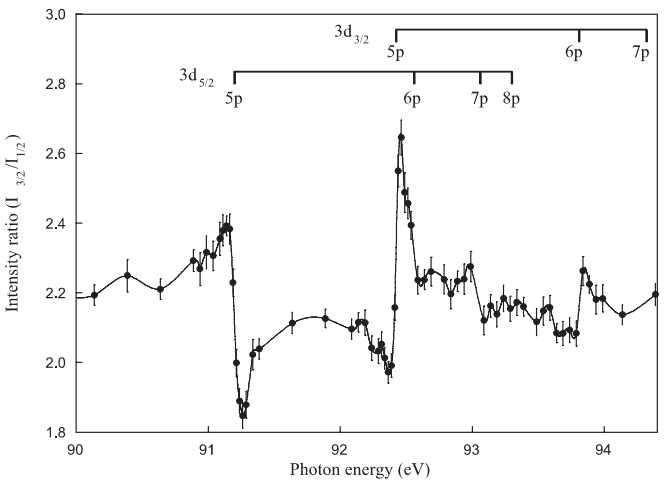

FIG. 6. Photon energy dependence of the experimental intensity ratios between the $4p_{3/2}$ and $4p_{1/2}$ photoelectrons of krypton.

minima of the intensity ratios are found in the vicinity of every resonant excitation energy.

V. CONCLUSIONS

The angular distribution of the Kr $4p$ photoelectrons was studied with the method of angle-resolved electron spectroscopy in the photon energy range of the $(3d)^{-1} \rightarrow np$ resonant excitations and a theoretical estimation was worked out for the description of the photoionization and excitation processes. The experimental dipole and nondipole anisotropy parameters were determined separately for the spin-orbit components. The measured dipole parameters were compared with the present model calculations. Both the measurement and the theoretical estimation show that the angular distribution of photoelectrons is influenced by the excitation processes. The difference between the shape of the measured and calculated dipole anisotropy parameters demonstrates the presence of interference between the direct ionization and the resonantly excited participator Auger decay processes. Similar effects were observed also for the γ nondipole anisotropy parameters where the interference is more pronounced.

A more precise theoretical model is necessary for the quantitative description of the experimental data and for understanding the observation in detail.

ACKNOWLEDGMENTS

The authors thank the DORIS III staff for providing excellent working conditions. This work was supported by the National Scientific Research Foundation and the National Office for Research and Technology of Hungary (NKTH-OTKA, Grant No. K67719) and by the European Community-Access to Research Infrastructure Action of the Improving Human Potential Program. Financial support by DESY is gratefully acknowledged.

[1] S. B. Whitfield, R. Wehlitz, H. R. Varma, T. Banerjee, P. C. Deshmukh, and S. T. Manson, J. Phys. B: At. Mol. Opt. Phys. **39**, L335 (2006).
[2] T. W. Gorczyca and F. Robicheaux, Phys. Rev. A **60**, 1216 (1999).
[3] S. Ricz, J. Nikkinen, R. Sankari, T. Ricsóka, Á. Kövér, D. Varga, S. Fritzsche, H. Aksela, and S. Aksela, Phys. Rev. A **72**, 014701 (2005).
[4] R. Reininger and V. Saile, Nucl. Instrum. Methods A **288**, 343 (1990).
[5] A. R. B. de Castro and R. Reininger, Rev. Sci. Instrum. **63**, 1317 (1992).
[6] T. Möller, Synchrotron Radiation News **6**, 16 (1993).
[7] C. U. S. Larsson, A. Beutler, O. Björneholm, F. Federmann, U. Hahn, A. Rieck, S. Verbin, and T. Möller, Nucl. Instrum. Methods A **337**, 603 (1994).
[8] O. Hemmers, G. Fisher, P. Glans, D. L. Hansen, H. Wang, S. B. Whitfield, R. Wehlitz, J. C. Levin, I. A. Sellin, R. C. C. Perera, E. W. B. Dias, H. S. Chakraborty, P. C. Deshmukh, S. T. Manson, and D. W. Lindle, J. Phys. B: At. Mol. Phys. **30**, L727 (1997).
[9] S. Ricz, Á. Kövér, M. Jurvansuu, D. Varga, J. Molnár, and S. Aksela, Phys. Rev. A **65**, 042707 (2002).
[10] A. Derevianko, W. R. Johnson, and K. T. Cheng, At. Data Nucl. Data Tables **73**, 153 (1999).
[11] M. Ya. Amusia, A. S. Baltenkov, L. V. Chernysheva, Z. Felfli, and A. Z. Msezane, Phys. Rev. A **63**, 052506 (2001).
[12] J. W. Cooper, Phys. Rev. A **47**, 1841 (1993).
[13] David J. Kennedy and S. T. Manson, Phys. Rev. A **5**, 227 (1972).
[14] H. K. Tseng, R. H. Pratt, S. Yu, and A. Ron, Phys. Rev. A **17**, 1061 (1978).
[15] V. L. Jacobs, J. Phys. B: At. Mol. Phys. **5**, 2257 (1972).
[16] *Handbook of Mathematical Functions*, edited by M. Abramowitz and I. A. Stegun, National Bureau of Standards (US) Applied Mathematics Series, Vol. 55 (US GPO, Washington, DC, 1964), p. 537.
[17] G. C. King, M. Tronc, F. H. Read, and R. C. Bradford, J. Phys. B **10**, 2479 (1977).
[18] S. Aksela, H. Aksela, M. Levasalmi, K. H. Tan, and G. M. Bancroft, Phys. Rev. A **36**, 3449 (1987).
[19] J. Tulkki, S. Aksela, H. Aksela, E. Shigemasa, A. Yagishita, and Y. Furusawa, Phys. Rev. A **45**, 4640 (1992).
[20] K.-N. Huang, W. R. Johnson, and K. T. Cheng, At. Data Nucl. Data Tables **26**, 33 (1981).
[21] A. F. Starace, Phys. Rev. A **3**, 1242 (1971).
[22] T. Banerjee, P. C. Deshmukh, and S. T. Manson, J. Phys. Conf. Ser. **80**, 012001 (2007).
[23] B. Krässig, E. P. Kanter, S. H. Southworth, R. Guillemin, O. Hemmers, D. W. Lindle, R. Wehlitz, and N. L. S. Martin, Phys. Rev. Lett. **88**, 203002 (2002).
[24] V. K. Dolmatov and S. T. Manson, Phys. Rev. A **74**, 032705 (2006).
[25] R. D. Cowan, *Theory of Atomic Structure and Spectra* (University of California Press, Berkeley, Los Angeles, 1981).
[26] Zhen-Sheng Yuan, Lin-Fan Zhu, Xiao-Jing Liu, Wen-Bin Li, Hua-Dong Cheng, Jian-Min Sun, and Ke-Zun Xu, Phys. Rev. A **71**, 064701 (2005).
[27] S. Ricz, R. Sankari, Á. Kövér, M. Jurvansuu, D. Varga, J. Nikkinen, T. Ricsóka, H. Aksela, and S. Aksela, Phys. Rev. A **67**, 012712 (2003).
[28] O. Hemmers, R. Guillemin, E. P. Kanter, B. Krässig, D. W. Lindle, S. H. Southworth, R. Wehlitz, J. Baker, A. Hudson, M. Lotrakul, D. Rolles, W. C. Stolte, I. C. Tran, A. Wolska, S. W. Yu, M. Ya. Amusia, K. T. Cheng, L. V. Chernysheva, W. R. Johnson, and S. T. Manson, Phys. Rev. Lett. **91**, 053002 (2003).